Kinetics and Catalysis, Vol. 42, No. 3, 2001, pp. 418–431. Translated from Kinetika i Kataliz, Vol. 42, No. 3, 2001, pp. 464–478.

Energetics of C–C Bond Scission in Ethane Hydrogenolysis: A Theoretical Study of Possible Intermediates and Reaction Pathways

A. V. Zeigarnik * and O. N. Myatkovskaya **

** Zelinskii Institute of Organic Chemistry, Russian Academy of Sciences, Moscow, 119992 Russia*

*** All-Russia Research Institute of Chemical Technology, Moscow, 115230 Russia*

Received February 22, 2000

Abstract—C–C bond scission steps, which are often considered as rate-determining in ethane hydrogenolysis, are studied by the Unity Bond Index–Quadratic Exponential UBI–QEP method. The binding energies of atomic carbon with Group VIII and IB metal surfaces Ni(111), Pd(111), Pt(111), Rh(111), Ru(001), Ir(111), Fe(110), Cu(111), and Au(111) are estimated using experimental data on the adsorption of various species on these surfaces. These estimates are corrected using data from density functional theory (DFT) on the adsorption heats of the CH_x species. Metal surfaces are arranged in the following series according to the binding strength of a carbon atom: Cu(111) < Au(111) < Pd(111) < Ru(001) ≈ Pt(111) < Ni(111) ≈ Rh(111) < Ir(111) < Fe(110). The values of chemisorption heats range from 121 kcal/mol for Au(111) to 193 kcal/mol for Fe(110). The activity of these surfaces toward C–C bond scission increases in the same series. The results of this work suggest that the most probable C–C bond scission precursors are ethyl, ethylidyne, adsorbed acetylene, CH_2CH, CH_2C, and CHC. Theoretical data obtained by different methods are compared and found to agree well with each other. An overview of experimental data on ethane hydrogenolysis mechanisms is given.

OVERVIEW OF EXPERIMENTAL DATA

The general mechanism of ethane hydrogenolysis (the Sinfelt–Taylor mechanism), which is proposed by most researchers includes the following main steps [1–3]:

(1) Chemisorption of H_2;

(2) Dehydrogenation of ethane on the catalyst surface to form adsorbed C_2H_x species;

(3) C–C bond scission in C_2H_x (x = 5–0) to form the CH_y species (y = 3–0);

(4) Hydrogenation of CH_y to form methane, which then desorbs from the surface.

The most frequent assumption is that the C–C bond scission step is rate-determining and that other steps are at pseudoequilibrium [2, 3]. Therefore, any C_2H_x or CH_y species is at equilibrium with either the reactants or the products of the reaction:

$$C_2H_6 + (6 - x)z \rightleftharpoons C_2H_xz_{6-x} + 3 - 0.5x)H_2, \quad \text{(I)}$$

$$CH_yz_{4-y} + 2 - 0.5y)H_2 \rightleftharpoons CH_4 + (4 - y)z, \quad \text{(II)}$$

where z is an adsorption site.

Sinfelt generalized ethane hydrogenolysis data in [1]. One of the main arguments in favor of the above mechanism is that hydrocarbons are chemisorbed on metal surfaces and form gaseous hydrogen at temperatures much lower than those required for hydrogenolysis. This fact indicates that C–H bonds are much more reactive than C–C bonds, although the latter are ~10 kcal/mol weaker. Factors that determine the heights of activation barriers are not only enthalpies of bond breaking but also binding energies (adsorption heats) of intermediate species with metal surfaces.

Analyzing the data on ethane hydrogenolysis within the framework of the above mechanism, Sinfelt came to a conclusion that, for different transition metals supported in SiO_2, the number of hydrogen atoms in the C_2H_x species that break C–C bonds is different [1, 4, 5]:

Metal	Co	Ni, Ru, Os, Ir	Rh, Pd, Pt
x	4	2	0

This analysis assumed the absence of competition between hydrogen and ethane for surface sites. This assumption was claimed to be contradictory to experimental observations and criticized by Boudart [6].

Mahaffy and Hansen [7] studied ethane hydrogenolysis on iridium films over wide ranges of the partial pressures of each reactant at 80–205°C. They assumed that hydrogen atoms and hydrocarbon fragments are adsorbed on the active sites of the same type. Mahaffy and Hansen proposed a mechanism according to which adsorbed ethyl and Hz are formed. The C–C bond in ethyl is cleaned under the action of Hz. A competing

0023-1584/01/4203-0418$25.00 © 2001 MAIK “Nauka / Interperiodica”

step is further ethyl dehydrogenation via α-elimination to form ethylidene:

$$\begin{aligned}
&(1)\ CH_3CH_{3(gas)} + 2z \rightleftharpoons CH_3CH_2z + Hz,\\
&(2)\ H_2 + 2z \rightleftharpoons 2Hz,\\
&(3)\ CH_3CH_2z + z \rightleftharpoons CH_3{-}CHz + Hz, \qquad \text{(III)}\\
&(4)\ CH_3CH_2z + Hz \rightleftharpoons 2CH_3z,\\
&(5)\ CH_3z + Hz \rightleftharpoons CH_{4(gas)} + 2z.
\end{aligned}$$

Experiments show that the concentration of methyl on the iridium surface can be neglected, because it is small compared to the concentrations of ethyl and ethylidene. According to data on H–D exchange in ethane, equilibrium is not achieved in steps (1)–(3) and (5). The authors [7] mentioned though that deuterium exchange was investigated briefly. They also found that ethylene poisons the catalyst surface and inhibits hydrogenolysis, whereas ethylidene is observed on the surface, but its effect is less significant. Thus, the proposed mechanism differs substantially from the Sinfelt–Taylor mechanism, which is assumed most frequently.

Guczi *et al.* [8] studied ethane hydrogenolysis catalyzed by nickel powder at 170–320°C at various partial pressures of ethane and hydrogen, as well as H–D exchange in ethane and methane. Their data are consistent with the Sinfelt–Taylor mechanism, and the C–C bond scission (the rate-determining step) occurs in more dehydrogenated species than C_2H_4(ads).

More recently, Gudkov *et al.* [9] studied ethane hydrogenolysis on Pt/SiO_2 and $Pt–Fe/SiO_2$ at 250–350°C and different ratios of the partial pressures of ethane and hydrogen. The authors assumed that C–C bond scission is a rate-determining step, but the number of hydrogen atoms in C_2H_x(ads) and the apparent activation energy depend on the ratio between the partial pressures of ethane and hydrogen. In hydrogen excess, the C–C bond is cleaved in CH_3CH_2(ads), whereas in ethane excess this occurs in CHCH(ads). Other steps are at pseudoequilibrium. Gudkov *et al*. [9] noted that the apparent activation energy strongly depends on the conditions of its measurement. The authors did not exclude the possibility of C–C bond scission in other adsorbed fragments, but they consider that CH_3CH_2(ads) and CHCH(ads) are the most important.

Interesting data were obtained for the Ni/Al_2O_3 catalyst [10]. Tanaka *et al*. advanced three hypotheses on the rate-determining step, which can be reactions of types (2), (3), and (4) in the Sinfelt–Taylor mechanism above. They carried out several experiments on (a) ethane hydrogenolysis on pure nickel surface, (b) ethane hydrogenolysis on the carbon-deposited surface (carbon was deposited on the surface by admitting CO before the main reaction), (c) ethane self-hydrogenolysis without adding hydrogen, and (d) ethylene hydrogenation together with ethane hydrogenolysis. Experimental data obtained in [10] suggest that the rate-determining step is C–C bond scission. It was shown that self-hydrogenolysis occurs with an induction period and accelerates substantially when hydrogen is added; then, it returns to the rate observed after the induction period before adding hydrogen. According to the data obtained with labeled CO, most of carbide-like carbon is hydrogenated to form methane and the rest of it does not decelerate the hydrogenolysis at 200°C. Broadly speaking, carbide and non-carbide phases of carbon behave differently. The authors summarized their findings by proposing the following mechanism. Ethane is dehydrogenated to form C_2 fragments on the surface, which slowly decompose into the CH_x fragments ($x > 0$). The latter is rapidly hydrogenated to form methane. CO and some of ethane molecules form carbide-like carbon, which is hydrogenated to methane somewhat more slowly than CH_x, but this process is still fast. The other portion of carbon (the non-carbide phase) formed from CO or methane is hydrogenated very slowly to form methane.

Zaera and Somorjai [11a] studied ethane hydrogenolysis and deuterium exchange on the Pt(111) single-crystal surface at 200–350°C and atmospheric pressure. The apparent activation energies for these two processes are 34 and 19 kcal/mol, respectively. The distribution of deuterated products had a *U*-like shape with maxima at d_1- and d_6-ethane (as well as on supported platinum catalysts, foils, and films). Low-energy electron diffraction (LEED) and thermal desorption spectroscopy were used to detect the presence of ethylidyne CH_3C on the catalyst surface. The rate of hydrogenolysis was found to be three orders of magnitude lower than the rate of deuterium exchange. This allowed Zaera and Somorjai to conclude that the steps preceding C–C bond scission are not rate-determining. The authors assumed that hydrogenolysis and partly deuterium exchange occur via a common intermediate, which is ethylidyne. Step (IV) is assumed to be rate-determining:

$$z_3CCH_3 + 4z \longrightarrow 2z_3CH + Hz. \qquad \text{(IV)}$$

This reaction can hardly be a single kinetic step. Its detailed mechanism may differ. One of the variants is the cleavage of a bond in ethylidyne and hydrogen exchange between two C_1 fragments. Another mechanism is ethylidyne dehydrogenation, C–C bond scission and further hydrogenation of carbide. Other variants are also possible.

Salmeron and Somorjai [11b] studied acetylene and ethylene on the Pt(111) surface. After their partial desorption these hydrocarbons started to dissociate and evolve hydrogen into the gas phase in portions. Therefore, hydrogen peaks were observed at several temperatures, which corresponded to certain apparent activation energies. For acetylene, four peaks were observed: 219 ± 5°C (E_a ~ 21 kcal/mol), ~277°C (E_a ~ 33 kcal/mol), ~366°C (E_a ~ 39 kcal/mol), ~440°C (E_a ~ 44 kcal/mol). In the case of ethylene, these four were supplemented with an additional peak at ~24°C (E_a ~ 18 kcal/mol). Salmeron and Somorjai proposed to interpret their find-

ings from the standpoint of possible occurrence of the reactions

$$C_xH_y \longrightarrow C_xH_{y-1} + 1/2H_{2(gas)}, \qquad (V)$$

and each reaction of this sort corresponds to a certain hydrogen desorption peak. Reaction (V) includes C–H bond scission and hydrogen recombination. Isomerization reactions are also possible. Because four peaks were observed for acetylene, Salmeron and Somorjai conjectured (taking into account other data) that C–C bond is cleaved at 219–440°C and vinylidene $CH_2{=}Cz_2$ is formed. Fragments that are formed cleave C–H bonds.

Salmeron and Somorjai's study [11b] shows that the C–C bond is cleaved at certain rates in several C_2 fragments rather than in one in the studied temperature range. The additional peak for ethylene can be due to the formation of ethylidyne and further C–H bond dissociation in it.

Chen and Goodwin [12] studied ethane hydrogenolysis on Ru/SiO_2 at 160–180°C by steady-state isotopic transient response kinetic analysis (SSITKA). Their results showed that the surface coverage of C_2 fragments is much lower than for C_1 fragments, although the latter are more reactive. The C–C bond scission is the slowest step in this system. The coverage by C_2 intermediates does not change with an increase in temperature, whereas the coverage by C_1 fragments increases. The authors postulated that the C–C bond scission step is as follows:

$$CH_3CH_2z + Hz \rightleftharpoons 2CH_3z. \qquad (VI)$$

Smale and King [13] assumed that the C–C bond is cleaved in the fragment with the stoichiometry C_2H_3 and that this step is rate-determining in the case of Ru/SiO_2.

Engstrom and Goodman [14] studied the hydrogenolysis of ethane and other saturated hydrocarbons on the low-index plane surfaces Ir(111) and Ir(110)-(1×2) at 177–427°C. They showed that the activation energies on these two surfaces differ substantially and that the mechanisms for them are different, but both of them are of the Sinfelt–Taylor type. Two temperature ranges can be identified, which are characterized by different apparent activation energies and preexponential factors for each of these planes. The authors connect the values of the preexponential factor and the stoichiometry of C_2 intermediates where the C–C bond is cleaved: the higher the dehydrogenation degree of the C_2 fragment, the higher the value of the preexponential factor. Engstrom and Goodman [14] believed that, in the case of the close-packed Ir(111) surface, the most probable intermediate where the C–C bond is cleaved is zCH_2CH_2z. In the case of the rougher surface Ir(110)-(1×2), on which high-coordination adsorption sites are available, z_2CHCHz_2 is formed which is bound to four adsorption sites. Partial coverages with hydrocarbon fragments were observed on both surfaces after the reaction. The addition of hydrogen only results in the formation of methane. A kinetic model derived from the Sinfelt–Taylor mechanism described well the kinetics over a wide range of temperatures and ethane and hydrogen partial pressures. This study shed some light on the main sources of structure sensitivity observed in hydrogenolysis. Substantial difference in the apparent activation energies for different temperature regions assumes the formation of several (rather than one) intermediates in which the C–C bond is cleaved. The idea that the C–C bond is cleaved in only one type of fragments is oversimplification, and good kinetic description is accidental in this case.

Frennet *et al.* [15] criticized the idea that the C–C bond scission is a rate-determining step on all metal surfaces, except Fe and Ru (Sinfelt's hypotheses). They supposed that the hydrogenation of C_1 fragments can also be rate-determining. The authors studied deuterium exchange in methane and summarized their findings and literature data as follows:

(1) Deuterium exchange in ethane always occurs at lower temperatures than hydrogenolysis does (except for Fe and Co).

(2) The rates of deuterium exchange in ethane and hydrogenolysis are very close on W, Ni, Rh, Ru, Re, and Pd. The rate of hydrogenolysis is somewhat lower on Ni, Re, and Pd and somewhat higher on Rh, Ru, and W.

(3) Deuterium exchange in methane is much faster on Fe, Co, and Cu, for which methane adsorption is very slow or does not occur at all (Cu).

(4) In the case of platinum, hydrogenolysis is slower than deuterium exchange.

According to Frennet *et al.* [15], these data suggest that the formation of methane in hydrogenolysis cannot be excluded as a rate-determining step, and that the rate-determining step can differ depending on the metal surface.

Dumesic and co-workers [16] carried out a series of mechanistic studies on ethane hydrogenolysis over Pt, Pd, Ir, and Co catalysts supported on SiO_2. They proposed the following mechanism:

$$(1)\ H_2 + 2z \rightleftharpoons 2Hz,$$

$$(2)\ CH_3{-}CH_3 + 2z \rightleftharpoons CH_3{-}CH_2z + Hz,$$

$$(3)\ CH_3{-}CH_2z + 2z \rightleftharpoons Hz + zCH_2{-}CH_2z,$$

$$(4)\ zCH_2{-}CH_2z + 2z \rightleftharpoons Hz + z_2CH{-}CH_2z,$$

$$(5)\ z_2CH{-}CH_2z + 2z \rightleftharpoons Hz + z_2CH{-}CHz_2,$$

$$(6)\ zCH_2{-}CH_2z + 2z \rightleftharpoons 2CH_2z_2, \qquad (VII)$$

$$(7)\ z_2CH{-}Ch_2z + 2z \rightleftharpoons CH_2z_2 + 2CHz_3,$$

$$(8)\ z_2CH{-}CHz_2 + 2z \rightleftharpoons 2CHz_3,$$

$$(9)\ CHz_3 + Hz \rightleftharpoons 2z + CH_2z_2,$$

$$(10)\ CH_2z_2 + Hz \rightleftharpoons 2z + CH_3z,$$

$$(11)\ CH_3z + Hz \rightleftharpoons 2z + CH_4.$$

This mechanism assumes that the C–C bond is cleaved in three fragments: $–CH_2–CH_2–$, $=CH–CH_2–$, and $=CH–CH=$. The authors considered three routes: route A (steps 1–3, 6, 10, and 11), route B (steps 1–4, 7, and 9–11), route C (steps 1–5 and 8–11). It was found that route C (the formation of $CHz_2–CHz_2$ before C–C bond scission) does not work. Routes A and B can dominate depending on the metal and reaction conditions. The activation energies estimated using the unity bond index–quadratic exponential potential (UBI–QEP) method are shown in Table 1.

Further modeling of ethane hydrogenolysis was carried out using density functional theory (DFT) calculations [2, 17]. In our opinion, the data of that work are unreliable. For instance, they agree with microcalorimetric measurements, which are not unambiguously interpretable and which overestimate chemisorption heats and underestimate the activation energies of C–C bond scission.

Rodriguez and Goodman [18] studied ethane hydrogenolysis on Pt(111) at T = 277–367°C, $P_{C_2H_4}$ = 0.5–4 torr, and P_{H_2} = 80–270 torr. They found that the C–C bond is cleaved in the adsorbates with the stoichiometry C_2H_4 and C_2H_3 (possibly in ethylidyne). This agrees with [11] but contradicts Sinfelt's data, according to which the number of hydrogen atoms in the case of Pt/SiO_2 is zero [1, 5].

Martin reported data for Ni/SiO_2 [19], which also contradict Sinfelt's findings. Martin believes that ethane is completely dehydrogenated on nickel before the C–C bond breaks. The addition of copper decelerates the process due to nickel site blocking or because of simple dilution of active nickel sites by inactive copper sites.

Wang *et al.* [20] obtained the apparent activation energies for C–C bond scission in the hydrogenolysis of ethane, ethylene, and acetylene on Ir and Pt supported on η-Al_2O_3. In the case of iridium, the apparent activation energies for the hydrogenolysis of these three compounds were found to be the same accurate to 1 kcal/mol (36 kcal/mol for ethane and ethylene and 37 kcal/mol for acetylene). In the case of platinum, the apparent activation energy is the same for acetylene and ethane (53 and 54 kcal/mol, respectively) and 17 kcal/mol lower for ethylene. Based on these data, the authors concluded that C_2H_2(ads) is a common intermediate in all three processes. The C–C bond breaks in this intermediate on iridium. In the case of platinum, the process is less clear: either C_2H_2 is further dehydrogenated or isomerized to ethylidyne in which the C–C bond breaks.

Ko and Garten [21] published data on strong metal–support interactions. They studied ethane hydrogenolysis on Fe, Co, Ni, Ru, Rh, Pd, Os, Ir, and Pt supported on TiO_2 and compared the results with Sinfelt's data [1, 5] for the same metals supported on SiO_2. It is interesting that not only metal activity depends on support, but also the degree of dehydrogenation in the fragments where the C–C bond breaks differs for TiO_2 and SiO_2 if the data are analyzed in the same manner (Table 2). The authors reported two series of specific activities for the Group VIII metals one of which corresponds to SiO_2 (Sinfelt's data):

Os > Ru > Ni > Rh > Ir > Co > Fe > Pt > Pd,

and the other corresponds to TiO_2 (Ko and Garten's data [21]):

Ru > Os > Rh > Ni > Ir > Co > Pd > Pt ~ Fe.

In both cases, Ru, Os, Rh, and Ni are the most active and Co, Fe, Pt, and Pd are less active. Iridium is moderately active. These data are valid for supported catalysts. For single-crystal surfaces, the picture is different. According to data generalized by Rodriguez and Goodman [22], the activity (in terms of the turnover numbers) decreases in the series

Ir(110)-(1 × 2) > Ir(111) > Ru(001) > Ni(100) >Re(001) > Ni(111) > W(100) > Pt(111).

Iridium in this series becomes more active than nickel and ruthenium. Platinum remains the least active surface.

PROBLEM STATEMENT

The above overview shows that the C–C bond scission in surface compounds plays an important role in

Table 1. Activation energies (in kcal/mol) of C–C bond scission in various species according to [16]

Metal (reaction)	$CH_2CH_2z \longrightarrow 2CH_2z$	$CHCH_2z \longrightarrow CH_2z + CHz$	$CHCHz \longrightarrow 2CHz$
Pt (forward)	28.3	30.4	24.3
Pt (reverse)	27.7	25.6	31.7
Ir (forward)	25.9	28.0	21.9
Ir (reverse)	28.1	26.0	32.1
Pd (forward)	28.5	30.6	24.5
Pd (reverse)	27.5	25.4	31.5
Co (forward)	27.7	29.8	23.7
Co (reverse)	26.3	24.2	30.3

hydrogenolysis process. Whether or not these steps are rate-determining, it is interesting to trace the trends in activation energies across different transition metals and C_2 fragments. With this goal, we used the UBI–QEP method [23, 24]. The general calculation scheme was as follows:

(I) Using published experimental data, we estimated the binding energies of atomic carbon to low-index single-crystal planes of transition metals and compared them to data obtained by other methods.

(II) Using the data obtained at the first stage, we calculated the chemisorption heats of C_1–C_2 molecules and radicals on these surfaces.

(III) Using the data obtained at the second stage, we calculated the activation energies of C–C bond scission.

In all calculations, we assumed that the surface is clean (free from adsorbates). The same condition was valid for the initial experimental data.

CALCULATION SCHEME

The main source of the estimates of atomic carbon binding energies Q_C is data on CO chemisorption heats (Q_{CO}). The metal–carbon bond energy D_{MC} ($D_{MC} = Q_{0C}$) and the heat of adsorption Q_{CO} are related by the following formula:

$$Q_{CO} = \frac{(Q_{0C})^2}{Q_{0C} + D_{CO}}, \quad (1)$$

where D_{CO} is the C–O bond strength (257 kcal/mol); D_{MC} is related with Q_C by the formula

$$Q_{0C} = \frac{Q_C}{(2 - 1/n)}, \quad (2)$$

where n is the number of metal atoms bound to the atom A. In the case of atomic carbon adsorbed on the (111) fcc or (001) hcp lattice surface, $n = 3$.

In the general case,

$$Q_{0A} = \frac{Q_A}{(2 - 1/n)}, \quad (3)$$

where Q_{0A} and Q_A is the metal–A bond energy and the binding energy (chemisorption heat) of atom A.

For monocoordinated chemisorbed molecules AB that are perpendicular to the metal surface and bound to it via the atom À, there are several calculation schemes depending on the assumed binding strength to the metal surface.

In the case of strong binding of an adsorbate X (X = CH_3CH, CH_3C, CH_2, CH) via the atom A (in our case A = C) the equation

$$Q_X = Q_A^2/(Q_A + D_{AB}), \quad (4)$$

is used, where D_{AB} is the sum of the energies of the bonds between the atom that binds X to the surface (the contact atom) and the rest of adsorbed molecule. For CH_3CH, CH_3C, CH_2, and CH, D_{AB} is 173, 83, 183, and 81 kcal/mol, respectively; $Q_A = Q_C$. The data on bond energies are taken from [25].

In the case of medium-strength binding [23, 24], the formula

$$Q_X = 0.5\left(\frac{Q_{0A}^2}{Q_{0A}/n + D_{AB}} + \frac{Q_A^2}{Q_A + D_{AB}}\right), \quad (5)$$

is used. X = CH_3CH_2 and CH_3, D_{AB} = 283 and 293 kcal/mol, respectively.

The binding strengths of the AB molecules bound to the surface via atoms A and B (M–A···B-M). The formula [23, 24]

$$Q_X = \frac{ab(a + b) + D_{AB}(a - b)^2}{ab + D_{AB}(a + b)}, \quad (6)$$

is used for the calculation, where

$$a = Q_{0A}^2(Q_{0A} + 2Q_{0B})/(Q_{0A} + Q_{0B})^2 \quad (7)$$

and

$$b = Q_{0B}^2(Q_{0B} + 2Q_{0A})/(Q_{0A} + Q_{0B})^2. \quad (8)$$

In Eq. (6), D_{AB} is the energy of C–C bond: $D_{CH_2–CH}$ = 157, $D_{CH_2–C}$ = 165, $D_{CH=C}$ = 178 kcal/mol [23]). The values of Q_{0A} and Q_{0B} in formulas (7) and (8) are determined by the equation (in our case, A and B are carbon atoms)

$$Q_{0B} = \frac{Q_{0C}^2}{Q_{0C} + D_i}, \quad (9)$$

where D_i is energy required to cleave the bonds between the contact atoms and "free" atoms in the fragment A or B. The values of D_i (kcal/mol) for different adsorbates that take into account the distribution of bond energies in the molecules are given below [23]: D_{CH_2} = 183 kcal/mol and D_{CH} = 81 kcal/mol.

For homonuclear adsorbates A_2 (–CH=CH–, –C≡C–, and $–CH_2–CH_2–$) Eq. (6) can be simplified:

$$Q_{A_2} = \frac{9Q_{0A}^2}{6Q_{0A} + 16D_{A_2}}. \quad (10)$$

Table 2. Stoichiometry of species in which C–C bond scission occurs on different metals and supports in ethane hydrogenolysis

Support	Metal			
	Ni	Ru	Rh	Pd
SiO_2 [4]	C_2H_2	C_2H_2	C_2	C_2
TiO_2 [21]	C_2H_4	C_2H_2	C_2	C_2H_2

For CH_2CH_2, CHCH, and CC, D_{A_2} is the energy of a bond between CH_2, CH, or C and the respective remaining part of the molecule in the gas phase: $D_{CH_2-CH_2} = 355$, $D_{CH=CH} = 311$, $D_{CH=CH} = 145$ kcal/mol; $Q_{0A} = Q_{0C}$ is the bond energy of the contact atom.

The UBI–QEP method allows one to calculate the activation energies of reactions. To calculate the activation energy of the dissociation reaction

$$AB_{ads} \longrightarrow A_{ads} + B_{ads} \quad \text{(VIII)}$$

the equation

$$E = 0.5[\Delta H + Q_A Q_B/(Q_A + Q_B)], \quad (11)$$

is used in which ΔH is the reaction enthalpy on the metal surface calculated from the thermodynamic cycle desorption–gas-phase reaction–adsorption:

$$\Delta H = Q_{AB} + D - Q_A - Q_B. \quad (12)$$

In this equation, D is the enthalpy of the analogous gas-phase reaction estimated from bond energies:

$$D = D_{AB} - D_A - D_B. \quad (13)$$

The activation energy of the reverse reaction is calculated from the condition

$$E_{reverse} = E_{forward} - \Delta H. \quad (14)$$

If the activation energy was negative, then we introduced thermodynamic correction: this activation energy is set to zero and the activation energy of the reverse reaction is set equal to the reaction enthalpy.

RESULTS OF CALCULATION

Carbon Chemisorption Heats

Cu(111). For Cu(111), we know only one experimental value related to Q_C. This is chemisorption heat of carbon monoxide $Q_{CO} = 11.9$ kcal/mol [26]. This value corresponds to $Q_C = 103$ kcal/mol. Other data are also available, but they do not refer to the zero coverage of the surface, which is used in this work. The Cu(100) surface is the closest to Cu(111), for which the following values are known: $Q_{CO} = 13.2 \pm 0.3$ kcal/mol [27] and $Q_{CO} = 13.5$ kcal/mol [28]. Data for the (100) plane can also be used, but with care, since ethane hydrogenolysis is a structure-sensitive reaction [29]. Here we assumed that Q_C for Cu(111) calculated as a mean of three values of binding energies of atomic carbon obtained using formula (1) and three experimental values of the CO adsorption heat: $Q_C = 107.1$ kcal/mol.

Ni(111). In most UBI–QEP calculations, it is assumed for Ni(111) that $Q_C = 171$ kcal/mol [23, 24, 30–33]. This is a "calibrated" value close to the experimental value for Ni(100): $Q_C = 169$ kcal/mol [34]. It was reported for Ni(111), that $Q_C = 160$ kcal/mol [34]. We will show below that the higher the binding energy of atomic carbon, the lower the activation energy of C–C bond scission. Thus, the fact that Ni(100) is more active in ethane hydrogenolysis [29] agrees well with the higher binding energy of carbon on Ni(100) and contradicts the idea that the same value of Q_C can be used for both Ni(111) and Ni(100).

For CO/Ni(111), the following values of the chemisorption heat were reported: 29.4 [35], 35.6 [36], 31 [37, 38], 30.3 [39], and 27 kcal/mol [40]. On the average, they correspond to $Q_C = 176$ kcal/mol.

About the same chemisorption heats were observed for CO/Ni(100): 26 [41], 30.3 [42], 30.8 [43, 44], 26 [45], 29.1 [37], 27.4 [46], 28.4 [47], and 32.9 kcal/mol [48]. They give the average value $Q_C = 170$ kcal/mol, which is close to the experimental one. The value $Q_{C_2H_4} = 12$ for Ni(100) [49, 50] gives a substantially lower value of the carbon binding energy: $Q_C = 152$ kcal/mol.

If we take all the experimental values for Ni(111) and Ni(100) and obtain the values of Q_C using formulas (1), (2), and (10), then the mean value is 170 kcal/mol. We adopted this value assuming that the structure sensitivity can be neglected in our calculations and consider that we deal with surfaces consisting of the (111) and (100) planes. This assumption is rational taking into account that the sensitivity of the Q_C value to the errors in Q_{CO}. A difference of 1.5 kcal/mol in Q_{CO} translates into a difference of ~5 kcal/mol in Q_C if we deal with the heats of the order considered above.

Pd(111). For Pd(111), we took only three very close values for Q_{CO}: 34 [51], 33.9 [52], and 35.3 kcal/mol [53]. The values for CO/Pd(100) are noticeably higher and we had to ignore them. The average value obtained by formulas (1) and (2) is $Q_C = 188$ kcal/mol.

Pt(111). For Pt(111), we took only the Q_{CO} values 26 [54], 32.3 [55], 33 [56, 57], 29.2 [58], and 34.9 kcal/mol [59] and analogous values obtained for Pt(100): 32 [60, 61] and 27.4 [62]. There are also some chemisorption heat data for hydrocarbons and radicals on this surface, but they gave either unbelievably low values of Q_C or seemed unreliable. The average value obtained for Pt(111) is $Q_C = 177$ kcal/mol.

Ru(001). For this surface, four experimental values are known: $Q_{CO} = 29$ kcal/mol [63], $Q_{CO} = 28$ kcal/mol [64], $Q_{C_2H_2} = 11.6$ kcal/mol [65], and $Q_{C_2H_4} = 10$–11 kcal/mol [66]. The two latter values correspond to substantially lower values of carbon binding energy and contradict to each other. Hence, we excluded them from consideration taking into account that the main body of calculations were based on Q_{CO}. The average value obtained for this surface is $Q_C = 168$ kcal/mol.

Rh(111). The only usable value that we had was $Q_{CO} = 30$ kcal/mol [67]. This value corresponds to $Q_C = 174$ kcal/mol. Of course, the use of a single value is unreliable and requires further refining as new data will appear.

Ir(111). For Ir(111) and Ir(100), we know three values of Q_{CO}: 35±1 [68], 34.1 [69], and 35.8 kcal/mol [70].

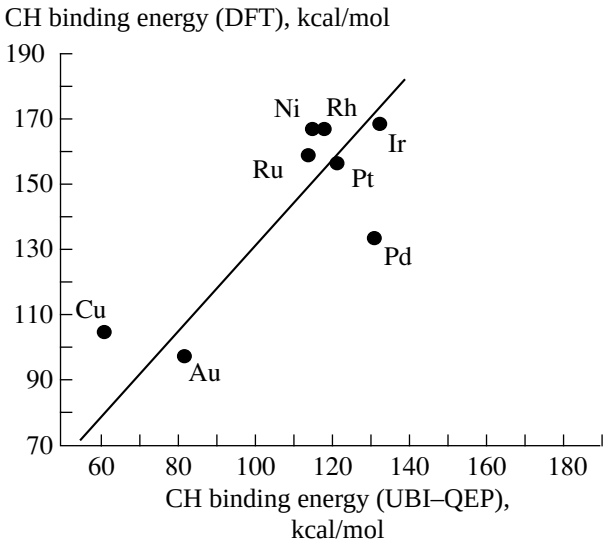

Fig. 1. Correlation plot of chemisorption heats obtained by the DFT and UBI–QEP methods.

The average value obtained with these data is Q_C = 190 kcal/mol.

Fe(110). The only usable experimental value for Fe(110) is Q_{CO} = 35.8 kcal/mol [71] giving Q_C = 193 kcal/mol.

Au(111). The data for Au(111) was based on Q_{CH_3} = 30 kcal/mol [32]: Q_C = 131 kcal/mol.

Thus, we obtained the values of Q_C corresponding to different surfaces. These data are summarized in Table 3. Usually, calculations are compared to experimental data assuming that the experiment is a reliable source of information and the calculation is only a model, which reflects the reality to a certain degree. In our opinion, both experiment and calculation may be in error, and there are many sources for such errors. The binding energies calculated above reflect experimental data available to date. These data would be more reliable if one would manage to correlate them with some physically sensible theoretical indices that characterize the metal–carbon bond strength on the above surfaces.

Unfortunately we know of no absolutely reliable theoretical data on the metal–carbon binding energies for Group VIII and IB metals. The most complete set of data can be found in [72, 73]. In these works the chemisorption heats of CH_x were calculated using density functional theory for the (111) surfaces of Ru, Os, Ir, Rh, Ni, Pd, Pt, Cu, Ag, and Au using the bond energies estimates by the transition state method. The VWN–B–P functional was used (Vosko–Wilk–Nusair's correction/Becke's gradient correction/Perdew gradient correction). Although these data are inexact, they are rather plausible. The absolute values of calculated binding energies of atomic carbon on Group IB metals are lower than analogous values for CH. Therefore, we used only the values of Q_{CH}. The hollow position of CH between three metal atoms calculated in [72, 73] was the most stable (the surface was modeled by the two-layer (3,7)-clusters):

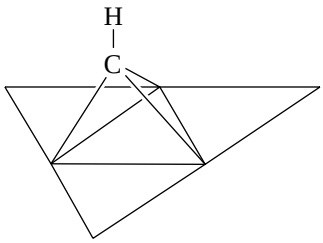

Data were corrected as follows. We calculated the binding energies of CH using the formula (4) and data obtained for Q_C. Then, we constructed a correlation plot with the CH chemisorption heats obtained by the DFT and UBI–QEP methods on the axes (Fig. 1). The latter values corresponded the results of experiments.

Because it is *a priori* unknown which of the data are more reliable we took the values corresponding to the intercepts obtained by dropping perpendiculars on the trend line from the points corresponding to different metals. The values thus obtained compromise with the experiment and theory. Then, we calculated Q_C back from the newly obtained balanced value (Table 3).

In further calculations we used both initial and corrected data.

Chemisorption Heats of Adsorbed Molecules and Radicals

Chemisorption heats were calculated using formulas (1)–(10). The results are summarized in Tables 4 and 5 for initial and corrected data, respectively. The values of chemisorption heats for ethane were not calculated by the UBI–QEP method. For Au(111), we took the experimental value [74]. For Cu(111), the value was obtained by the extrapolation of the plot of physical adsorption heat on Cu(100) vs. carbon chain length in

Table 3. Carbon chemisorption heats

Q_C, kcal/mol	Cu(111)	Ni(111)	Pd(111)	Pt(111)	Rh(111)	Ru(001)	Ir(111)	Fe(110)	Au(111)
Q_C^*	107	170	188	177	174	168	183	193	131
Q_C^{**}	122	179	168	176	180	174	187		127

* Obtained from experimental data.

** Obtained after DFT correction [72, 73].

Table 4. Chemisorption heats of CH_x and C_2H_x calculated by the UBI–QEP method using experimental values

Species	D*	Q, kcal/mol								
		Cu(111)	Ni(111)	Pd(111)	Pt(111)	Rh(111)	Ru(001)	Ir(111)	Fe(110)	Au(111)
C	–	107.1	170.1	188.0	176.9	173.5	168.3	189.6	192.5	131.2
CH	81	61.0	115.2	131.4	121.3	118.3	113.6	132.8	135.5	81.1
CH_2	183	39.5	81.9	95.3	87.0	84.4	80.6	96.5	98.7	54.8
CH_3	293	20.9	47.2	56.0	50.5	48.8	46.3	56.8	56.5	30.0
CH_3CH_3	674	6.2	7.7	7.7	7.6	7.0	8.8	7.7	8.7	5.7
CH_3–CH_2	576	21.5	48.4	57.4	51.7	50.0	47.5	58.2	57.9	30.8
CH_3–CH	466	41.0	84.3	97.9	89.4	86.9	83.0	99.1	101.4	56.6
CH_2–CH_2	538	6.1	14.9	18.0	16.1	15.5	14.6	18.3	17.2	9.1
CH_3–C	376	60.3	114.3	130.4	120.4	117.4	112.7	131.9	134.5	80.4
CH_2–CH	421	7.3	14.5	17.2	15.5	15.0	14.3	17.4	16.4	9.8
CH_2–C	348	46.0	59.3	62.7	60.6	60.0	59.0	63.0	67.8	51.6
CH=CH	392	6.9	16.8	20.3	18.1	17.4	16.4	20.6	19.3	10.2
CH=C	259	28.8	36.9	40.0	38.0	37.4	36.6	40.2	39.1	31.5
C≡C	145	13.7	32.0	38.2	34.3	33.1	31.4	38.8	36.5	20.0

* D is the sum bond energies in the corresponding species.

Table 5. Chemisorption heats of CH_x and C_2H_x calculated by the UBI–QEP method using corrected values

Species	D*	Q, kcal/mol							
		Cu(111)	Ni(111)	Pd(111)	Pt(111)	Rh(111)	Ru(001)	Ir(111)	Au(111)
C	–	122.1	179.1	168.2	176.2	180.3	174.3	187.1	126.8
CH	81	73.4	123.3	113.5	120.7	124.4	119.0	130.6	77.4
CH_2	183	48.9	88.6	80.6	86.4	89.5	85.0	94.6	51.9
CH_3	293	26.4	51.5	46.3	50.1	52.1	49.2	55.5	28.2
CH_3–CH_3	674	6.2	7.7	7.7	7.6	7.0	8.8	7.7	5.7
CH_3–CH_2	576	27.1	52.8	47.4	51.4	53.4	50.4	56.9	29.0
CH_3–CH	466	50.5	91.1	82.9	88.9	92.0	87.5	97.2	53.6
CH_2–CH_2	538	7.9	16.4	14.6	15.9	16.6	15.6	17.9	8.5
CH_3–C	376	72.7	122.4	112.6	119.8	123.5	118.1	129.6	76.6
CH_2–CH	421	8.8	15.8	14.3	15.4	16.0	15.1	17.0	9.3
CH_2–C	348	49.6	61.0	59.0	60.5	61.2	60.1	62.5	50.6
CH=CH	392	8.9	18.5	16.4	17.9	18.7	17.6	20.1	9.6
CH=C	259	30.4	38.4	36.6	37.9	38.6	37.6	39.8	31.0
C≡C	145	17.5	35.1	31.3	34.0	35.5	33.4	37.9	18.8

* D is the sum bond energies in the corresponding species (kcal/mol).

normal alkanes [74, 75]. For Pt(111), we took the experimental value [74, 76, 77]. For C_2H_6/Rh(111), we took a value that is 1 kcal/mol higher than the corresponding experimental value for CH_4/Rh(poly) [78]. For Ru(001), the value was obtained by the extrapolation of the plot of physical adsorption heat on Ru(001) vs. carbon chain length in normal alkanes [75, 79]. For Ir(111), the experimental value was used [80]. For Ni(111) and Pd(111), we used the same value as for Pt(111) and Ir(111). For Fe(110), the value was taken 1 kcal/mol higher than for Ni(111).

The heats of chemisorption increase with an increase in the values of the metal–carbon bond ener-

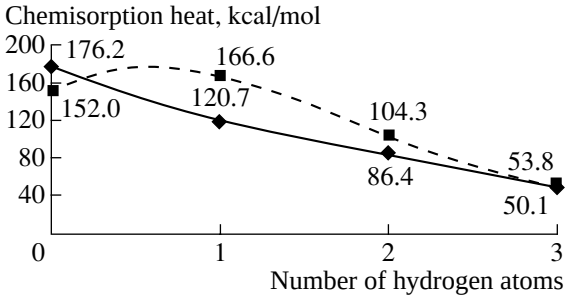

Fig. 2. Trends in the changes of chemisorption heats for CH_x/Pt(111), calculated by UBI–QEP (solid line) and DFT (dashed line) [81] methods.

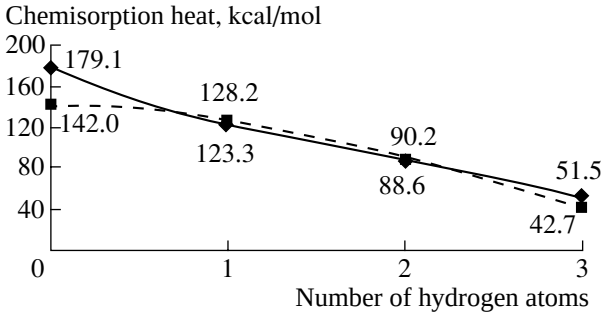

Fig. 3. Trends in the changes of chemisorption heats for CH_x/Ni(111), calculated by UBI–QEP (solid line) and DFT (dashed line) [82] methods.

gies. The chemisorption heats of CH, CH_3C, CH_2, and CH_3CH exhibit the most pronounced growth. That is, these chemisorption heats are the most sensitive to the errors in the values of metal–carbon bond strengths.

It is hard to compare the UBI–QEP data obtained in this work with data obtained by other methods because the absolute values can be unreliable even in the case of high-level calculations. However, some comparisons are possible. Thus, for instance Kua and Goddard [81] obtained data for single-layer clusters consisting of eight metal atoms by DFT (B3LYP) calculation and the interstitial electron surface model that they have developed earlier. Single-layer clusters of ten atoms were also considered. The chemisorption heats of adsorbates in the most stable configurations CH_3 (on-top), CH_2 (bridge), and CH_3 (hollow) differ from the UBI–QEP data and even follow a different trend (see Fig. 2). According to DFT, the chemisorption heat is equal to the number of bonds between a carbon atom and the surface (53 ± 3 kcal/mol per each Pt–C bond). This trend contradicts to the bond-order conservation idea. Also, we find it dubious that carbon binds to the platinum surface more weakly than methylidyne.

Other chemisorption heats also differ considerably. In the case of quantum mechanical calculations, the binding energy increases more rapidly with and increase in the number of bonds with the surface than in the case of UBI–QEP calculations.

It is also interesting to compare our (corrected) results for Ni(111) with data obtained in [82] by the DFT method for three-layer (7,3,3)-clusters of Ni with 13 atoms (Fig. 3). It can be seen that the shapes of curves are the same as for platinum, but the curves are closer to each other. It is interesting that according to DFT calculation, the most stable is the tree-centered) hollow position of CH_2 rather than bridging (two-centered) one. Somewhat more accurate results were obtained for the C/Ni(111) system where the surface was modeled by a five-layer slab [83]. The refined value of the carbon binding energy is 156 kcal/mol. For CH/Ni(111), the refined value is 150 kcal/mol [84]. Data obtained in [85] for CH_3/Ni(111) agree well with those reported in [82].

The agreement of calculations by the MRCCI method [86] for Ni(111) using the clusters consisting of 10–20 atoms and data obtained in this work (Fig. 4) is nearly ideal, but the chemisorption heat for C/Ni(111) was not calculated in [86]. Based on the data for CH_x/Ni(100) obtained by the MRCCI method in [86], we may assume that the difference will be the most pronounced for $x = 0$, where we expect that the chemisorption heat will be approximately 145 kcal/mol.

For Pd(111), DFT calculation was performed using 2–3-layer slabs and a surface coverage of 1/3 [87]. Although our data correspond to the zero-coverage limit, the difference in the chemisorption heats is small. Figure 5 compares the results obtained by different methods. Here, we also see analogous shapes of the curves.

Analysis of curves in Figs. 2–5 showed that DFT and UBI–QEP data are described by different approximating curves. In both cases, the curves can be described by third-order polynomials with alternating negative and positive coefficients but alterations exhibit "phase displacement." Therefore, the best fit is for $x = 1$ and 2. The difference is moderate for $x = 3$, but it is the most pronounced for $x = 0$. Therefore, the most accurate results for the chemisorption heats of other radicals and molecule can be obtained by the UBI–QEP method if it uses Q_C that is calculated from DFT's Q_{CH_x} ($x = 1, 2$).

In all cases considered here except Pt(111), our calculated data agree well with other calculations. Let us additionally analyze the data from [81]. If we take two chemisorption heat values for CH/Pt(111) and CH_2/Pt(111) from [81], and calculate the chemisorption heat for C/Pt(111) by the UBI–QEP method, then we obtain Q_C ranging from 199 to 225 kcal/mol, which contradicts the experiment: in this case platinum becomes the most active metal, whereas it is the one of the least active metals in Group VIII in ethane hydrogenolysis.

When this study was already completed, we found a paper by Frese [88], in which carbon binding energies

were estimated by the semiempirical polar covalence model (PCM). This method was proposed by Sanders and adapted by Frese for adsorption on surfaces. There is no quantitative agreement between UBI–QEP and PCM methods, which predict completely different bond energies, but the qualitative agreement is excellent: in our calculations the carbon binding energy increases in the series

$$Pd < Ru \approx Pt < Ni < Ir < Fe.$$

In the case of PCM, the activity series is

$$Pd < Pt \approx Ru < Ni \approx Ir < Fe.$$

Activation Energies of C–C bond Scission

Activation energies were calculated using formulas (11)–(14). The data for corrected values of carbon binding energies are summarized in Table 6. If the activity of metals in ethane hydrogenolysis is estimated by the values of activation energies (which is not fully correct), the metals are arranged in the following series in which the activity decreases:

$$Fe > Ir > Pd > Pt > Rh > Ni \approx Ru > Au > Cu.$$

After correction, this series transforms as follows

$$Fe > Ir > Rh \approx Ni > Pt \approx Ru > Pd > Au > Cu.$$

After iron, for which the activity is not determined by the C–C bond scission steps in hydrogenolysis, iridium is the most active metal in both cases, which is consistent with the activity series reported in [22]. In the case of iron, carbon phases are probably formed very intensively and this suppresses iron activity [21]. Low activities of Group IB metals in ethane hydrogenolysis predicted by our calculation agree with experiments. According to our calculated data, nickel is more active than ruthenium, and this conflicts with the experiment. Therefore, either the activation energy of C–C bond scission is a poor criterion or carbon chemisorption heats were incorrectly estimated (most likely for Ru). The latter hypothesis is more plausible because the apparent chemisorption strength of ruthenium is usually higher than that of nickel. The relatively high activity of platinum also contradicts experimental findings, and this can also be attributed to the incorrect position of ruthenium in the activity series.

Both chemisorption heats and the activation energies of steps largely depend on the carbon binding strength on the metal surface. Figure 6 illustrates this dependence. It is interesting that the activation energies of C–C bond scission in intermediates where both carbon atoms are bound to the surface are more sensitive to the carbon binding strength than in the case of intermediates that are bound via one atom. This means that if one manages to prove that the bond scission in ethylidyne, ethylidene, or ethyl is an important step for ethane hydrogenolysis on one metal, then this step should be taken into account when considering the reaction on similar metals. However, if it is necessary to take into account C–C bond scission in C_2H_2(ads) or

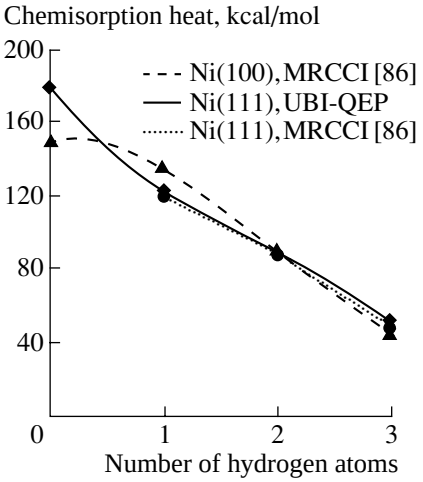

Fig. 4. Trends in the changes of chemisorption heats for CH_x/Ni(111) and CH_x/Ni(100), calculated by UBI–QEP and MRCCI [86] methods.

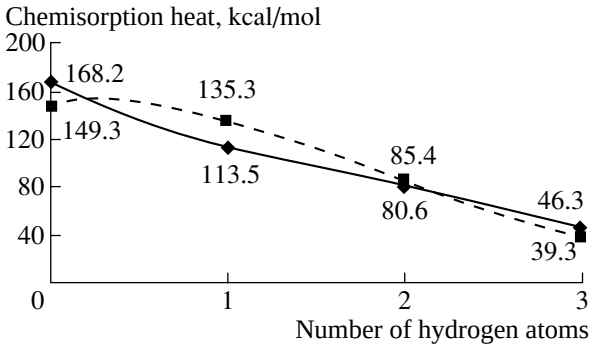

Fig. 5. Trends in the changes of chemisorption heats for CH_x/Pd(111), calculated by UBI–QEP (solid line) and DFT (dashed line) [87] methods.

C_2H_4(ads) for one metal, then it does not mean that these steps will occur on other metals.

Other important conclusions can be drawn if we take into account that the carbon chemisorption heats for Group VIII and IB metals range from 120 to 200 kcal/mol and that the steps with activation energies of 50–60 kcal/mol cannot occur. Therefore, we can restrict ourselves to considering a small region in Fig. 6. In this region, C–C bond scission in intermediates that do not contain hydrogen occur with zero activation energies on all metals. It is likely that the complete dehydrogenation of ethane does not occur because most experimental data are consistent with the hypothesis that C–C bond scission is a rate-determining step. The activation energy of C–C bond scission in ethylidene is about the same as in analogous steps with ethyl. According to experimental data, ethyl transforms to ethylidene very rapidly, especially at high temperatures. Therefore, the competition of C–C bond scission

Table 6. Activation energies and reaction enthalpies (kcal/mol)

Reaction*	*D***	Cu(111)	Ni(111)	Pd(111)	Pt(111)	Rh(111)	Ru(001)	Ir(111)	Au(111)
Activation energies of forward reactions									
$CH_3CH_3 \longrightarrow CH_3 + CH_3$	88	41.4	9.2	13.2	10.2	8.4	11.5	6.2	37.2
$CH_3CH_2 \longrightarrow CH_3 + CH_2$	100	51.9	22.6	25.0	23.3	22.4	23.7	20.9	48.9
$CH_3CH \longrightarrow CH_3 + CH$	92	42.7	22.3	24.0	22.7	22.1	23.0	21.0	40.0
$CH_2CH_2 \longrightarrow CH_2 + CH_2$	172	82.2	27.8	32.9	29.1	27.2	30.0	24.0	76.7
$CH_3C \longrightarrow CH_3 + C$	83	14.4	7.4	8.7	7.7	7.2	8.0	6.4	13.8
$CH_2CH \longrightarrow CH_2 + CH$	157	43.5	6.2	12.2	7.8	5.6	8.8	1.9	37.0
$CH_2C \longrightarrow CH_2 + C$	165	43.6	8.8	14.8	10.4	8.1	11.5	4.3	36.9
$CHCH \longrightarrow CH + CH$	230	92.1	31.8	38.1	33.4	31.1	34.5	27.1	84.8
$CHC \longrightarrow CH + C$	178	29.4	0.0	0.3	0.0	0.0	0.0	0.0	26.4
$CC \longrightarrow C + C$	145	0.0	0.0	0.0	0.0	0.0	0.0	0.0	0.0
Enthalpies									
$CH_3CH_3 \rightleftharpoons CH_3 + CH_3$	88	41.4	−7.4	3.2	−4.6	−9.2	−1.6	−15.4	37.2
$CH_3CH_2 \rightleftharpoons CH_3 + CH_2$	100	51.9	12.7	20.6	14.8	11.8	16.2	6.8	48.9
$CH_3CH \rightleftharpoons CH_3 + CH$	92	42.7	8.2	15.1	10.1	7.5	11.3	3.1	40.0
$CH_2CH_2 \rightleftharpoons CH_2 + CH_2$	172	82.2	11.3	25.5	15.1	9.7	17.5	0.7	76.7
$CH_3C \rightleftharpoons CH_3 + C$	83	7.2	−25.2	−18.8	−23.5	−26.0	−22.4	−30.0	4.6
$CH_2CH \rightleftharpoons CH_2 + CH$	157	43.5	−39.1	−22.8	−34.7	−40.9	−31.9	−51.1	37.0
$CH_2C \rightleftharpoons CH_2 + C$	165	43.6	−41.7	−24.8	−37.2	−43.6	−34.2	−54.2	36.9
$CHCH \rightleftharpoons CH + CH$	230	92.1	1.8	19.4	6.5	−0.1	9.6	−11.1	84.8
$CHC \rightleftharpoons CH + C$	178	12.9	−86.1	−67.2	−81.0	−88.1	−77.7	−99.9	4.8
$CC \rightleftharpoons C + C$	145	−81.7	−178.1	−160.1	−173.4	−180.1	−170.2	−191.3	−89.8
Activation energies of reverse reactions									
$CH_3 + CH_3 \longrightarrow CH_3CH_3$	88	0.0	16.6	10.0	14.8	17.7	13.1	21.6	0.0
$CH_3 + CH_2 \longrightarrow CH_3CH_2$	100	0.0	9.9	4.4	8.4	10.6	7.5	14.1	0.0
$CH_3 + CH \longrightarrow CH_3CH$	92	0.0	14.1	8.9	12.7	14.6	11.8	17.9	0.0
$CH_2 + CH_2 \longrightarrow CH_2CH_2$	172	0.0	16.5	7.4	14.1	17.5	12.5	23.3	0.0
$CH_3 + C \longrightarrow CH_3C$	83	7.3	32.6	27.6	31.3	33.2	30.4	36.4	9.3
$CH_2 + CH \longrightarrow CH_2CH$	157	0.0	45.3	35.0	42.6	46.5	40.7	53.0	0.0
$CH_2 + C \longrightarrow CH_2C$	165	0.0	50.5	39.6	47.6	51.7	45.7	58.5	0.0
$CH + CH \longrightarrow CHCH$	230	0.0	29.9	18.7	26.9	31.1	25.0	38.2	0.0
$CH + C \longrightarrow CHC$	178	16.5	86.1	67.5	81.0	88.1	77.7	99.9	21.6
$C + C \longrightarrow CC$	145	81.7	178.1	160.1	173.4	180.1	170.2	191.3	89.8

* All species are adsorbed on the surface.

** Energy of bond breaking.

steps in these two surface compounds will be determined by their surface concentrations. A similar picture is observed in the case of CH_2C(ads) and CH_2CH(ads). The dissociation of the C–C bond in CH_2CH_2(ads) can probably be excluded completely, assuming that the activation energy of this process is too high. At the same time, an analogous process with CHCH(ads) cannot be excluded. It can occur in the case of metals with

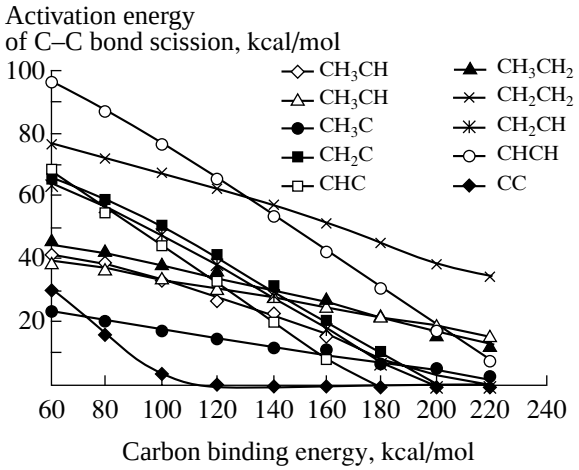

Fig. 6. Dependence of the activation energies of C–C bond scission in various surface intermediates on the carbon binding energy.

higher metal–carbon binding energies. Furthermore, in our calculations we did not take into account the possibility of four σ-bonds between C_2H_2 and the surface. For this type of adsorption, the C–C bond scission is more favorable. We should also exclude ethane as a possible candidate for C–C bond scission because of steric factors. Note that ethylidyne, whose surface concentration is usually very high, dissociates readily. This fact is hard to explain because the most stable configuration of ethylidyne is its perpendicular position relative to the surface, unlike many η^2-adsorbates considered here.

Thus, ethyl, ethylidyne, adsorbed acetylene, CH_2CH, CH_2C, and CHC are intermediates that are most important for the kinetic description of the process and that are theoretically most probable.

In all cases, the higher the metal–carbon binding energy, the more favorable is C–C bond scission, but the stability of surface species is also higher. Metals with higher adsorption strength are characterized by the formation of ethylidyne species and the like. These species block active sites and decrease the true activity of metals. Thus, there is some optimum for the metal–carbon binding strength near which adsorption is neither strong enough for efficient surface blocking nor weak enough for the activation energy of C–C bond scission to be high.

CONCLUSION

Thus, the UBI–QEP study of C–C bond scission, which is often considered as a rate-determining step in ethane hydrogenolysis, showed that metal surfaces can be arranged in the following series where the binding strength of carbon decreases Cu(111) < Au(111) < Pd(111) < Ru(001) ≈ Pt(111) < Ni(111) ≈ Rh(111) < Ir(111) < Fe(110). The values of atomic carbon chemisorption heats range from 122 kcal/mol for Au(111) to 193 kcal/mol for Fe(110). The activity of metal surfaces toward C–C bond scission increases in the same series. Therefore, the most probable intermediates in which C–C bond scission occurs are ethyl, ethylidyne, adsorbed acetylene, CH_2CH, CH_2C, and CHC. For surfaces with higher chemisorption strengths C–C bond scission steps may not be rate-determining and the true activity of these surfaces is not determined by the chemisorption strength. The data obtained in this work agree well with experimental data and data obtained by other calculations. We plan to focus our further efforts on refining the metal–carbon binding energies and on the modeling of ethane hydrogenolysis.

ACKNOWLEDGMENTS

We thank Irena Efremenko (Department of Chemical Engineering, Technion – Israel Institute of Technology, Haifa) for useful notes.

REFERENCES

1. Sinfelt, J.H., *Adv. Catal.*, 1973, vol. 23, p. 91.
2. Cortright, R.D., Watwe, R.M., Spiewak, B.E., and Dumesic, J.A., *Catal. Today*, 1999, vol. 53, no. 3, p. 395.
3. Bond, G.C., Hooper, A.D., Slaa, J.C., and Taylor, A.O., *J. Catal.*, 1996, vol. 163, no. 2, p. 319.
4. Sinfelt, J.H., *Catal. Rev.*, 1970, vol. 3, p. 175.
5. Sinfelt, J.H., *J. Catal.*, 1972, vol. 27, no. 3, p. 468.
6. Boudart, M., *AIChE J.*, 1972, vol. 18, p. 465.
7. Mahaffy, P. and Hansen, R.S., *J. Chem. Phys.*, 1979, vol. 71, no. 4, p. 1853.
8. Guczi, L., Gudkov, B.S., and Tetenyi, P., *J. Catal.*, 1972, vol. 24, no. 2, p. 187.
9. Gudkov, B.S., Guczi, L., and Tetenyi, P., *J. Catal.*, 1982, vol. 74, no. 2, p. 207.
10. Tanaka, K., Miyazaki, T., and Aomura, K., *J. Catal.*, 1983, vol. 81, no. 2, p. 328.
11. (a) Zaera, F. and Somorjai, G.A., *J. Phys. Chem.*, 1985, vol. 89, no. 15, p. 3211; (b) Salmeron, M. and Somorjai, G.A., *J. Phys. Chem.*, 1982, vol. 86, no. 3, p. 341.
12. Chen, B. and Goodwin, J.G., Jr., *J. Catal.*, 1995, vol. 154, no. 1, p. 1.
13. Smale, M.W. and King, T.S., *J. Catal.*, 1990, vol. 125, no. 2, p. 335.
14. Engstrom, J.R., Goodman, D.W., and Weinberg, W.H., *J. Am. Chem. Soc.*, 1988, vol. 110, no. 25, p. 8305.
15. Frennet, A., Degols, L., Lienard, G., and Crucq, A., *J. Catal.*, 1974, vol. 35, no. 1, p. 18.
16. Dumesic, J.A., Rudd, D.F., Aparicio, L.M., *et al.*, *The Microkinetics of Heterogeneous Catalysis*, Washington: American Chemical Society, 1993, Ch. 7.
17. Watwe, R.M., Spiewak, B.E., Cortright, R.D., and Dumesic, J.A., *J. Catal.*, 1998, vol. 180, no. 2, p. 184.
18. Rodriguez, J.A. and Goodman, D.W., *J. Phys. Chem.*, 1990, vol. 94, no. 13, p. 5342.
19. Martin, G.A., *J. Catal.*, 1979, vol. 60, no. 3, p. 345.
20. Wang, P.-K., Slichter, C.P., and Sinfelt, J.H., *J. Phys. Chem.*, 1990, vol. 94, no. 3, p. 1154.

21. Ko, E.I. and Garten, R.L., *J. Catal.*, 1981, vol. 68, no. 1, p. 233.
22. Rodriguez, J.A. and Coodman, D.W., *Surf. Sci. Rep.*, 1991, vol. 14, nos. 1–2, p. 1.
23. Shustorovich, E., *Adv. Catal.*, 1990, vol. 37, p. 101.
24. Shustorovich, E. and Sellers, H., *Surf. Sci. Rep.*, 1998, vol. 31, nos. 1–3, p. 1.
25. *CRC Handbook of Chemistry and Physics*, Robert, C.W., Ed., Boca Raton, FL: CRC, 1985–1986.
26. Hollins, P. and Pritchard, J., *Surf. Sci.*, 1979, vol. 89, nos. 1–3, p. 486.
27. Peterson, L.D. and Kevan, S.D., *J. Chem. Phys.*, 1991, vol. 94, no. 3, p. 2281.
28. Tracy, J.C., *J. Chem. Phys.*, 1972, vol. 56, no. 6, p. 2748.
29. Goodman, D.W., *Surf. Sci.*, 1982, vol. 123, no. 1, p. L697.
30. Shustorovich, E. and Bell, A.T., *Surf. Sci.*, 1991, vol. 248, no. 3, p. 359.
31. Shustorovich, E. and Bell, A.T., *Surf. Sci.*, 1991, vol. 253, nos. 1–3, p. 386.
32. Paredes-Oliveira, P., Patrito, E.M., and Sellers, H., *Surf. Sci.*, 1995, vol. 327, no. 3, p. 330.
33. Hei, M.J., Chen, H.B., Yi, J., *et al.*, *Surf. Sci.*, 1998, vol. 417, no. 1, p. 82.
34. Isett, L. and Blakeley, J.N., *Surf. Sci.*, 1975, vol. 47, no. 2, p. 645.
35. Christmann, K., Schober, O., and Ertl, G., *J. Chem. Phys.*, 1974, vol. 60, no. 12, p. 4719.
36. Ibach, H., Erley, W., and Wagner, H., *Surf. Sci.*, 1980, vol. 92, no. 1, p. 29.
37. Stuckless, J.T., Al-Sarraf, N., Wartnaby, C.E., and King, D.A., *J. Chem. Phys.*, 1993, vol. 99, no. 3, p. 2202.
38. Miller, J.B., Sidiqui, H.R., Gates, S.M., *et al.*, *J. Chem. Phys.*, 1987, vol. 87, no. 11, p. 6725.
39. Froitzheim, H. and Köhler, U., *Surf. Sci.*, 1987, vol. 188, nos. 1–2, p. 70.
40. *The Nature of the Surface Chemical Bond*, Rhodin, T.N. and Ertl, G., Eds., Amsterdam: Noth Holland, 1979.
41. Johnson, S. and Madix, R.J., *Surf. Sci.*, 1981, vol. 108, no. 1, p. 77.
42. Boszo, F., Ertl, G., Grunze, M., and Weiss, M., *Appl. Surf. Sci.*, 1977, vol. 1, no. 1, p. 103.
43. Bordoli, R.S., Vickerman, J.C., and Wolsteholm, J., *Surf. Sci.*, 1979, vol. 85, no. 2, p. 244.
44. Labohm, F., Engelen, C.W.R., Gijzeman, O.L.J., *et al.*, *J. Chem. Soc., Faraday Trans. 1*, 1982, vol. 78, p. 2435.
45. Klier, K., Zettlemoyer, A.C., and Leidheiser, H., Jr., *J. Chem. Phys.*, 1970, vol. 52, no. 2, p. 589.
46. Benziger, J.B. and Madix, R.J., *Surf. Sci.*, 1979, vol. 79, no. 2, p. 394.
47. Kiskinova, M. and Goodman, D.W., *Surf. Sci.*, 1981, vol. 108, no. 1, p. 64.
48. Koel, B.E., Peebles, D.E., and White, J.M., *Surf. Sci.*, 1983, vol. 125, no. 3, p. 709.
49. Tjandra, S. and Zaera, F., *Surf. Sci.*, 1993, vol. 289, no. 3, p. 255.
50. Tjandra, S. and Zaera, F., *Surf. Sci.*, 1995, vol. 322, nos. 1–3, p. 140.
51. Ertl, G. and Koch, J., *Z. Naturforsch. A*, 1970, vol. 25, no. 12, p. 1906.
52. Conrad, H., Ertl, G., Koch, J., and Latta, E.E., *Surf. Sci.*, 1974, vol. 43, no. 2, p. 462.
53. Voogt, E.H., Coulier, L., Gijzeman, O.L.J., and Geus, J.W., *J. Catal.*, 1997, vol. 169, no. 1, p. 359.
54. McCabe, R.W. and Schmidt, L.D., *Surf. Sci.*, 1977, vol. 66, no. 1, p. 101.
55. Ertl, G., Neumann, M., and Streit, K.M., *Surf. Sci.*, 1977, vol. 64, no. 2, p. 393.
56. Sexton, B.A., Rendulic, K.D., and Hughes, A.E., *Surf. Sci.*, 1982, vol. 121, no. 1, p. 181.
57. Shigeishi, R.A. and King, D.A., *Surf. Sci.*, 1976, vol. 58, no. 2, p. 379.
58. Lee, W.T., Ford, L., Blowers, P., *et al.*, *Surf. Sci.*, 1998, vol. 416, nos. 1–2, p. 141.
59. Campbell, C.T., Ertl, G., Kuipers, H., and Segner, J., *J. Chem. Phys.*, 1980, vol. 73, no. 11, p. 5862.
60. Barteau, M.A., Ko, E.I., and Madix, R.J., *Surf. Sci.*, 1981, vol. 102, no. 1, p. 99.
61. Küppers, J. and Michel, H., *J. Vac. Sci. Technol.*, 1976, vol. 13, p. 259.
62. Thiel, P.A., Behm, R.J., Norton, P.R., and Ertl, G., *J. Chem. Phys.*, 1983, vol. 78, no. 12, p. 7448.
63. Madey, T.E. and Menzel, D., *Jpn. J. Appl. Phys.*, 1974, suppl. 2, pt. 2, p. 841.
64. Reed, P.D., Comrie, C.M., and Lambert, R.M., *Surf. Sci.*, 1976, vol. 59, no. 1, p. 33.
65. Hills, M.M., Parmeter, J.E., Mullins, C.B., and Weinberg, W.H., *J. Am. Chem. Soc.*, 1986, vol. 108, no. 23, p. 3554.
66. Parmeter, J.E., Hills, M.M., and Weinberg, W.H., *J. Am. Chem. Soc.*, 1987, vol. 109, no. 1, p. 72.
67. Castner, D.G., Sexton, B.A., and Somorjai, G.A., *Surf. Sci.*, 1978, vol. 71, no. 3, p. 519.
68. Comrie, C.M. and Weinberg, W.H., *J. Chem. Phys.*, 1976, vol. 64, no. 1, p. 250.
69. Kuchaev, V.L., Nikitushina, L.M., and Temkin, M.I., *Kinet. Katal.*, 1974, vol. 15, no. 5, p. 1202.
70. Lauterbach, J., Boyle, R.W., Schick, M., *et al.*, *Surf. Sci.*, 1996, vol. 350, p. 32; Sushchikh, M., Lauterbach, J., and Weinberg, W.H., *Surf. Sci.*, 1997, vol. 393, p. 135.
71. Wedler, G. and Ruhmann, H., *Surf. Sci.*, 1982, vol. 121, no. 3, p. 464.
72. Au, C.-T., Ng, C.-F., and Liao, M.-S., *J. Catal.*, 1999, vol. 185, no. 1, p. 12.
73. Liao, M.-S. and Zhang, Q.-E., *J. Mol. Catal., A: Chem.*, 1998, vol. 136, no. 2, p. 185.
74. Wetterer, S.M., *Helium Atom Reflectivity Study of Physisorption and Chemisorption on Single Crystal Metal Surfaces, Ph.D. Thesis*, Princeton: Princeton Univ., 1998.
75. Kubota, J., Ichihara, S., Kondo, J.N., *et al.*, *Surf. Sci.*, 1996, vol. 357/358, p. 634.
76. McMaster, M.C., Arumainayagam, C.R., and Madix, R.J., *Chem. Phys.*, 1993, vol. 177, no. 2, p. 461.
77. Arumainayagam, C.R., Schoofs, G.R., McMaster, M.C., and Madix, R.J., *J. Phys. Chem.*, 1991, vol. 95, no. 3, p. 1041.
78. Brass, S.G. and Ehrlich, G., *Surf. Sci.*, 1987, vol. 187, no. 1, p. 21.

79. Brand, J.L., Arena, M.V., Deckert, A.A., and George, S.M., *J. Chem. Phys.*, 1990, vol. 92, no. 8, p. 5136.
80. Johnson, D.F. and Weinberg, W.H., *J. Chem. Phys.*, 1995, vol. 103, no. 13, p. 5833.
81. Kua, J. and Goddard III, W.A., *J. Chem. Phys. B*, 1998, vol. 102, no. 47, p. 942.
82. Burghgraef, H., Jansen, A.P.J., and van Santen, R.A., *Surf. Sci.*, 1995, vol. 324, nos. 2–3, p. 345.
83. Klinke II, D.J., Wilke S., and Broadbelt, L.J., *J. Catal.*, 1998, vol. 178, no. 2, p. 1998.
84. Klinke II, D.J., Dooling D.J., and Broadbelt L.J., *Surf. Sci.*, 1999, vol. 425, nos. 2–3, p. 334.
85. Michaelides, A. and Hu, P., *Surf. Sci.*, 1999, vol. 437, no. 3, p. 362.
86. Siegbahn, P.E.M. and Panas, I., *Surf. Sci.*, 1990, vol. 240, nos. 1–3, p. 37.
87. Paul, J.-F. and Sautet, P., *J. Phys. Chem. B.*, 1998, vol. 102, no. 9, p. 1678.
88. Frese, K.W., Jr., *Surf. Sci.*, 1987, vol. 182, nos. 1–2, p. 85.